Journal of Applied Polymer Science

Helium permeability of polymer materials as liners for composite overwrapped pressure vessels

Brendan R. Murray,[1,2] Sean B. Leen,[1] Christopher O. A. Semprimoschnig,[3] Conchúr M. Ó Brádaigh[4]

[1]Mechanical Engineering, National University of Ireland Galway, Ireland
[2]MaREI Centre, Environmental Research Institute, University College Cork, Ireland
[3]ESA-ESTEC, TEC-QTE, Materials Space Evaluation and Radiation Effects Section, The Netherlands
[4]Insitute for Materials and Processes, The University of Edinburgh, Scotland, UK
Correspondence to: B. R. Murray (E-mail: b.murray9@nuigalway.ie)

ABSTRACT: Polymers have been identified as replacement materials for metallic liners in composite overwrapped pressure vessels (COPVs) for future space launchers. PEEK, Nylon, and PVDF plastics formed from base powder grades have been permeability tested to determine their susceptibility to the diffusion of helium through flatwise panel cross sections. Permeability, diffusion, and solubility coefficients have been obtained for each material with PVDF and PA11 grades showing the lowest permeability coefficients and hence the best barrier properties to permeation. Crystallinity percentages and internal air void contents in the polymer samples have also been used to assess the differences in permeability between materials with an analysis of void dispersion effects given through X-ray CT scanning techniques. The measured permeability coefficients have been used to assess the ability of all materials tested to act as a functional polymer liner in a standard COPV with final leak rates predicted based on liner thicknesses and weights. © 2016 Wiley Periodicals, Inc. J. Appl. Polym. Sci. **2016**, *133*, 43675.

KEYWORDS: manufacturing; molding; thermoplastics; X-ray

Received 7 October 2015; accepted 22 March 2016
DOI: 10.1002/app.43675

INTRODUCTION

Composite overwrapped pressure vessels (COPVs) have become a critical component in satellite and space applications since their initial introduction in the early 1970s.[1,2] Their ability to store highly permeating fuels at high pressures under cryogenic conditions makes them an integral part of propulsion systems, breathing systems, and specialized research and analysis equipment aboard rockets, satellites, and spacecraft.[3–5] They have replaced traditional all-metal tanks due to their significant reduction in weight, dimensional flexibility, and inherent cost savings.[6,7]

While new materials and configurations have been developed for COPVs, the core design principles have remained unchanged. They consist of two distinct layers, the inner low-permeability liner and the outer high-strength fiber overwrap. The inner liner contains the fuel and limits permeation through the tank wall while the outer fiber overwrap absorbs the stresses generated by the high pressure fuel within.

Titanium has usually been the preferred liner material for high end applications. Its exceptional barrier properties, coupled with its good specific strength and resistance to chemical attack has made it a standard material for low permeability technologies with most satellite and spacecraft utilizing titanium lined COPVs exclusively.[8,9] The permeability coefficient of titanium is between 2.4×10^{-13} scc m^{-1} s^{-1} bar^{-1} and 3.5×10^{-14} scc m^{-1} s^{-1} bar^{-1} (titanium permeability coefficients calculated from leak rates for 0.5 mm thick tanks with surface areas of 1.0 m^2).[7,10] Aluminium materials have shown similarly low permeability characteristics with coefficients in the region of 7.1×10^{-12} scc m^{-1} s^{-1} bar^{-1}.[11]

The only drawback to titanium is its associated cost, whereby a 50 cm diameter liner can cost in the region of $90,000 due to precision machining operations and elevated material costs.[12] These high costs have restricted the use of COPVs in other fields of industry and so recent research has focused on developing alternative low cost liner materials.

Polymer materials have been identified as prospective replacements for metallic liners in future COPV structures. Their high barrier properties, light weight characteristics, and significantly lower cost make them an attractive alternative to their metallic counterparts. The cost of sending materials to space has been estimated to be almost \$11,000 kg^{-1}–\$20,000 kg^{-1} (€9,800 kg^{-1}–€17,800 kg^{-1} approximately) with the cost

Table I. Characteristics of Polymer Materials Tested

Polymer	Name	T_m (°C)	Dens. (g cm^{-3})	Avg. size (μm)	Proc. temp (°C)	x_c (%)
PEEK	1000P	343	1.30	630	380	44
	2000P	341	1.30	540	380	44
	150P	346	1.30	1800	380	42
	150PF	344	1.30	70	380	46
Nylon	PA11	187	1.05	330	240	23
	PA12	176	1.01	260	240	24
PVDF	PVDF	161	1.78	320	200	25

significantly affected by launch type and final orbital position of the payload, and so reducing the weight of inherent systems is a main priority for future launch designs.[13,14] A number of studies have already focused on the barrier properties of polymers in similar applications with PTFE, PFA, and PEEK exhibiting good barrier properties to gas permeation.[15–17] Polymer liner studies have also been applied directly to COPV structures with a myriad of polymer materials being tested to determine their overall permeability. Polyimides, nylons, and liquid crystal polymers have all been tested in these studies with initial results showing significant promise.[18–20]

These positive test results have allowed COPV technologies to progress toward the realization of a functional polymer liner, with AVIO and Astrium ST incorporating thermoplastic liners into new COPV structures.[21,22] These steps demonstrate an increasing trend toward the use of plastics in COPVs with a number of different polymers functioning as low permeability barrier materials.

While different processing methods have been used to manufacture the polymer liners mentioned such as blow injection moulding and plastic welding, the manufacturing methods utilized are quite capital intensive.[23] This has the effect of transferring the cost of liner formation to the tooling and does not significantly reduced the final cost of the liner itself. To this end, rotational moulding has been suggested as an alternative manufacturing method for low permeability liner production.

Rotational moulding is an inexpensive polymer processing method that produces hollow parts of uniform wall thickness using a specially ground powder material. Rotational moulds are inexpensive to produce and alter, as there is no use of pressure or centrifugal force, creating parts free of residual stresses.[24] The research presented here focuses on the testing of polymer materials, formed using rotational moulding techniques, to determine their permeability characteristics and suitability as liner materials in future COPV structures.

EXPERIMENTAL

Materials Tested

A number of polymers have been tested within this study to determine which exhibit the lowest permeation rates and are, therefore, possible candidate liner materials in future COPV liners. PEEK materials tested included VICTREX 150P and 150PF powder grades with EVONIK 1000P and 2000P powder grades also tested. The PA11 (ROTO11), PA12 (ARVO 950), and PVDF (2850) materials were supplied by Matrix Polymers and are based on their rotomoulding range of powder materials.

Differential scanning calorimetry following ASTM D3418 has been used to determine the melting temperature, T_m, of each material with the crystallinity, x_c, of the as-delivered powder polymer also analyzed.[25] Sieve tests following ASTM D1921 have been conducted to determine the average particle size of each powder material with the processing temperature range of each sample also quoted in Table I.[26] Samples were formed on a hot plate apparatus as this process has been shown to simulate rotational moulding conditions specifically in the area of void formation.[27–29] The hot plate allows for powder coalescence in a similar manner to that of the rotational moulding process, creating flat specimens with internal void contents which are representative of the rotomoulding process with similar heating conditions and rates.

Hot Plate Formation

The hot plate used in the formation of all samples consisted of a flat aluminium surface with a heating system embedded beneath the plate. The powder polymer was placed on the surface of the plate within a metal collar with an aluminium sheath

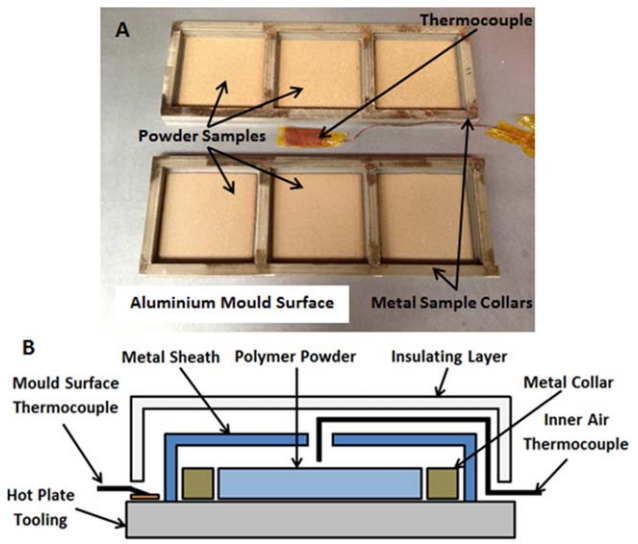

Figure 1. (a) Hot plate apparatus for polymer sheet formation with (b) a schematic representation of the sample forming process. [Color figure can be viewed in the online issue, which is available at wileyonlinelibrary.com.]

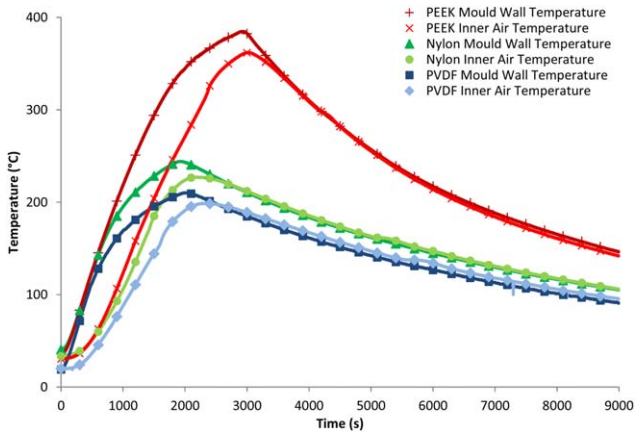

Figure 2. Heating cycles for the hot plate formed PEEK, Nylon and PVDF samples. [Color figure can be viewed in the online issue, which is available at wileyonlinelibrary.com.]

placed over the powder to protect the surface from contaminants, Figure 1. Thermocouples were attached to monitor the plate surface temperature and the inner air temperature and the entire plate was encased in a layer of insulation. The powder melts where it is in contact with the plate surface creating a moving front which propagates slowly up through the powder, melting the powder particles, and causing them to coalesce together. The temperature of the plate is held above the melting temperature of the polymer for a specific period of time and then disengaged to allow the molten melt to cool and solidify. The measured hot plate heating cycles for all samples have been included in Figure 2 showing both the mould surface and inner air temperatures. Three samples of each material were formed and tested for helium leak rates.

Processing Effects–Air Voids

This processing method creates air voids within the part due to the lack of applied pressure during sample formation. Air is circulating between the particles prior to heating and once the particles start to melt and coalesce together the circulating air is trapped beneath the surface causing void growth, Figure 3. This

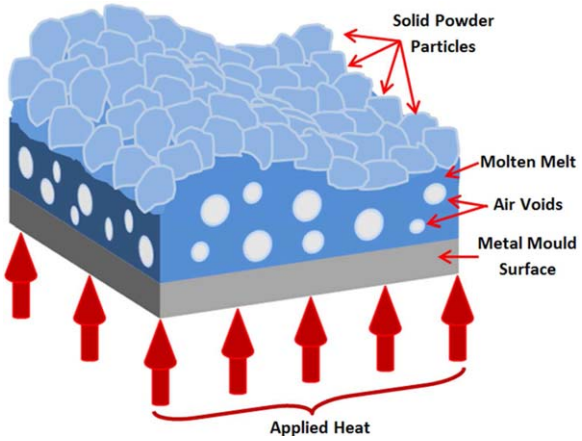

Figure 3. Bubble formation description for hot plate formed samples. [Color figure can be viewed in the online issue, which is available at wileyonlinelibrary.com.]

Table II. X-ray CT Nanotom Gun Settings for Image Capture

Parameter	Value
Timing (ms)	1000
Average	3
Skip	1
Binning	1
Sensitivity	2
V Sensor	1
Voltage (kV)	160
Current (μA)	28

inherent by-product of hot plate and rotomoulding manufacturing generates air void distributions in the part wall directly affecting permeability, as the air is significantly more permeable then the surrounding polymer material.[29]

X-ray CT scanning has been used on the tested polymer laminates to identify the void volume contents and void distributions in the polymer samples. The X-ray CT machine used here is a GE V/tome/X m300 with a Nanotom gun operating at a voltage of up to 160 kV, with other factors used quoted in Table II. A 20 mm × 20 mm sample of each material has been subjected to repeated X-ray imaging at varying orientations, giving a resolution of between 15–25 μm. These X-ray images were then reconstructed with the use of VGStudio MAX 2.2 software, rendering a 3D model of the polymer sample with the internal voids highlighted through the use of defect analysis software. The internal void volume fraction along with the average void size has been measured and used to assess the effects of voids and defects on each material's permeability.

Leak Rate Apparatus

The apparatus used to test leak rates through each polymer material follows the standard test method as outlined in ASTM D1434.[30] The sample is clamped between two chambers and a vacuum is applied to both sides of the sample. Once a sufficiently low vacuum has been achieved in the downstream chamber the helium leak detector (L200 Leybold Leak Detector) is engaged and measures the leak rate via a mass spectrometer. Research grade helium gas, with a purity of 99.999%, is then

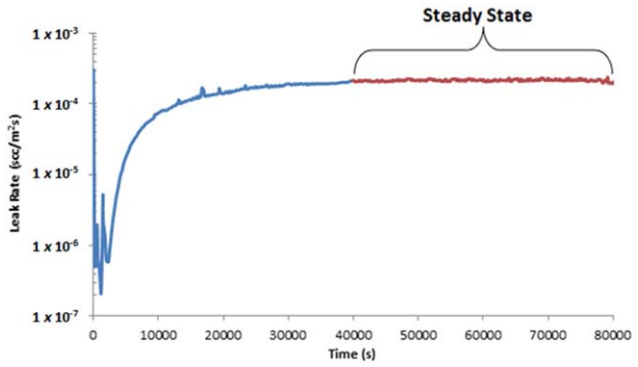

Figure 4. Typical leak rate output for a standard permeability test with steady state highlighted. [Color figure can be viewed in the online issue, which is available at wileyonlinelibrary.com.]

introduced into the upstream chamber at 1 bar (±20 mbar) and allowed to permeate through the sample.

Once the gas permeates through the sample, it is collected by the detector which outputs the leak rate results to "Leakware" software which monitors the leak rate over the test duration. A typical test can last anywhere from 12 to 48 hrs depending on the polymer tested and the sample thickness. This is to ensure that steady state conditions have been reached and the final leak rate is at a maximum value for that sample as indicated in Figure 4 by the horizontal portion of the graph.

Permeability Coefficients

The helium leak detector outputs the leak rate in units of mbar l^{-1} s^{-1}. Standard units for the leakage of helium for an entire COPV structures are scc s^{-1} which are obtained by multiplying the mbar l^{-1} s^{-1} output by 0.987.[31] This gives the standard leak rate through the sample but does not give sufficient detail about the sample's permeability coefficients. To obtain values for permeability, diffusion, and solubility coefficients the leak rate must be changed to a graph mapping the increase in the volume of gas passing through the sample over time.

The total volume of gas V that has passed through the sample at any time step can be calculated by adding together the volume of gas which has escaped at each corresponding time step from $t = 0$. Then, by using the relationship[32,33]:

$$V = PA\Delta pt/B \tag{1}$$

where A is the sample area (0.009499 m^2), Δp is the pressure difference across the sample (1 bar), t is the test time, and B is the sample thickness, the permeability coefficient P can be obtained by rearranging the equation and plotting $VB/A\Delta p$ versus t to obtain P as the slope of the linear portion of the line at steady state conditions as demonstrated in Figure 5.

The diffusion coefficient D can also be obtained from this graph by defining the time lag L as the point where a straight line fitted to the linear steady state portion of the graph in Figure 5 intercepts the time axis. This corresponds to the time taken for the diffusing gas to break through the sample and is governed by the relationship[32,33]:

$$L = B^2/6D \tag{2}$$

from which the diffusion coefficient, D, can be obtained. The solubility coefficient, S, is then calculated by dividing the permeability coefficient by the diffusion coefficient giving an overview of the relationship between the leak rate and the time taken to reach steady state conditions as outlined by[32]:

$$S = P/D \tag{3}$$

Fick's Law of Diffusion

While these coefficients are beneficial for comparing individual materials, the final leak rate J is the most important factor for liner studies. This is because COPV tanks are qualified against a maximum helium leak rate for the entire tank structure at the maximum expected operating pressure of the tank. The coefficients calculated from the experimental results can be used in conjunction with Fick's law of diffusion[32]:

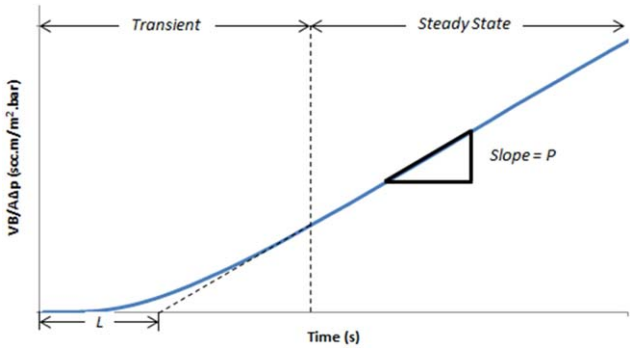

Figure 5. Sample graph to determine permeability coefficient and time lag. [Color figure can be viewed in the online issue, which is available at wileyonlinelibrary.com.]

$$J = -D\frac{\partial C}{\partial B} \tag{4}$$

where C is the concentration difference and all other symbols are as previously defined, thus determining the leak rate of each polymer sample at different thicknesses and pressures. The concentration, C, can be defined as the product of the solubility coefficient and the pressure difference across the sample and allows for the calculation of the leak rate J using the previously defined coefficients[34]:

$$C = S.\Delta p \tag{5}$$

The thickness of each sample will directly affect the final leak rate with thicker samples giving a lower leak rate for each material as $J \propto B^{-1}$. To this end, a comparison has been drawn between each material using Fick's law for specific thicknesses to obtain a true comparison between samples and to identify materials which meet the low leak rate requirements.

RESULTS AND DISCUSSION

Leak Rate Results

Table III shows the measured leak rates and subsequent calculations for permeability, diffusion, and solubility coefficients for each material tested. PVDF and PA11 have shown the lowest leak rates of around 7.0×10^{-5} scc m^{-2} s^{-1} followed by PA12 at around 1.3×10^{-4} scc m^{-2} s^{-1}. The PEEK grades have displayed higher leak rates in a range of 1.6×10^{-4} scc m^{-2} s^{-1} to 5.2×10^{-4} scc m^{-2} s^{-1}. The different PEEK grades show a significant difference in initial leak rates for similar materials with the EVONIK PEEK grades (1000P and 2000P) having a leak rate of nearly twice that of the VICTREX grades (150P and 150PF). This is not unexpected for the leak rate measurement as the VICTREX samples were twice as thick as their EVONIK counterparts and leak rate is thickness dependent.

The permeability coefficients of PA11 and PVDF are almost identical at less than 3.5×10^{-7} scc m^{-1} s^{-1} bar^{-1}. The PA12 and PEEK grades have all much higher values ranging from 6.5×10^{-7} to 12.0×10^{-7} scc m^{-1} s^{-1} bar^{-1}. The permeability coefficient is independent of part thickness and so the difference in permeability coefficient for the 2000P material from its PEEK counterparts cannot be explained by differences in part thickness. These permeability coefficients are significantly higher than those of the previously quoted metal liner materials, but

Table III. Experimental Results for Mass Flow Rates at Each Thickness with Permeability, Diffusion, and Solubility Coefficients Calculated for Each Material

Material	Grade	Thickness (mm)	Leak rate, J (10^{-5} scc m^{-2} s)	Permeability coefficient, P (10^{-7} scc m^{-1} s^{-1} bar^{-1})	Diffusion coefficient, D (10^{-11} m^2 s^{-1})	Solubility coefficient, S (10^3 scc m^{-3} bar^{-1})
PEEK	1000P	2.40	35.23	8.25	18.27	4.54
	2000P	2.13	52.27	11.67	18.63	6.50
	150P	3.13	23.47	7.34	9.60	7.69
	150PF	4.42	16.00	6.52	12.12	5.44
Nylon	PA11	5.75	6.27	3.36	23.93	1.41
	PA12	5.23	12.75	6.59	38.43	1.80
PVDF	PVDF	5.09	7.55	3.46	8.47	4.11

polymers are still capable of meeting the low permeability requirements of COPV applications as shown later.

The diffusion coefficients for the Nylon materials have settled at higher values of between 24 × 10^{-11} m^2 s^{-1} and 38 × 10^{-11} m^2 s^{-1} while the PEEK and PVDF materials have much lower values of 8.5 × 10^{-11} m^2 s^{-1} to 18.6 × 10^{-11} m^2 s^{-1}. This highlights the time taken for the gas molecules to pass through each material and shows that the PVDF and PEEK materials take significantly longer for steady state conditions to be reached. The solubility coefficient, which is a ratio between the permeability coefficient and diffusion coefficient, has switched these positions again with the Nylon materials having a lower coefficient at around 1.4 × 10^3 scc m^{-3} bar^{-1} while the PVDF and PEEK materials have higher values at 4.1 × 10^3 scc m^{-3} bar^{-1} to 7.7 × 10^3 scc m^{-3} bar^{-1}. While the results given for the measured coefficients are important, the permeability coefficient in the most prominent factor for permeation analyses as it also ranks materials in a manner which is independent of part thickness.

The crystallinity of the as-formed materials has also been assessed, with results presented in Figure 6. The crystallinity of a polymer material has been shown to have a direct effect on the permeability of a material with higher crystallinity percentages equating to a reduction in permeability.[35–38] The PEEK materials have crystallinity percentages around 30% while the Nylon materials have percentages around 20%. The crystallinity of the PVDF has risen considerably from its initial powder measurement in Table I with a 41.43% crystalline structure. The consistency of the crystallinity percentages in the PEEK materials can be explained by the use of the same cooling rate in the forming of all samples. The 150PF sample has the highest crystallinity of all PEEK samples tested at 33.79%, and also has the lowest permeability coefficient of all PEEK materials tested. Results for the 150P and 1000P materials are consistent with this as they have average crystallinity percentages of 31.65% and 30.31%, respectively, with correspondingly higher permeabilities. Although the 2000P material would be expected to have the lowest crystallinity, due to having the highest permeability, this is not the case as the 2000P material has an average crystallinity of 32.63%. An explanation for this is given in the section below on the basis of measured internal voids and defects affecting the permeability of the 2000P material.

Void Volume Fraction and Void Size Assessments

A comprehensive analysis of void volume fractions, V_f, and average void radii, R_v, was also conducted on all of the samples tested. X-ray CT imaging was used to determine the void volume fraction and average void radius in each material along

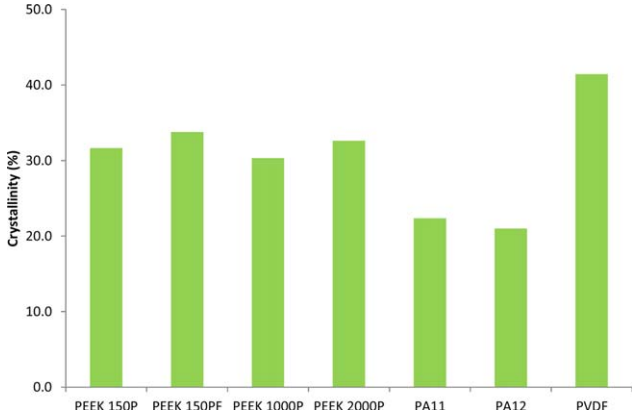

Figure 6. Crystallinity measurements of the hot plate formed polymer specimens. [Color figure can be viewed in the online issue, which is available at wileyonlinelibrary.com.]

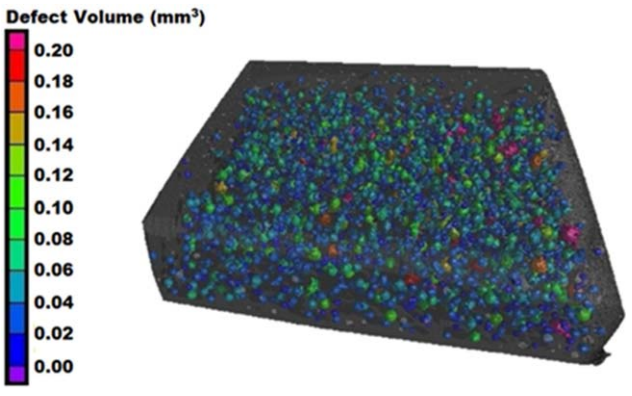

Figure 7. X-ray CT scan coupled with defect analysis software showcasing the internal voids in a PVDF sample. [Color figure can be viewed in the online issue, which is available at wileyonlinelibrary.com.]

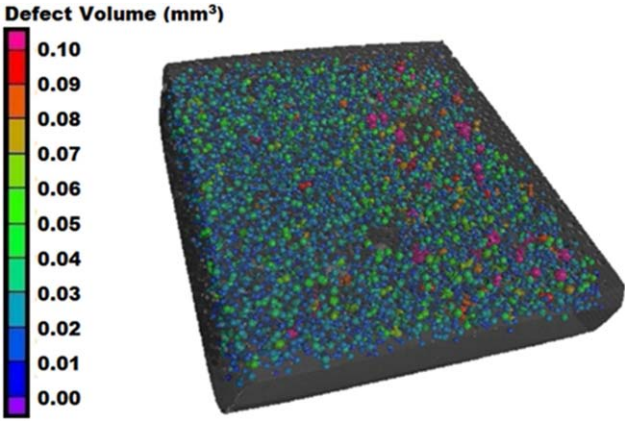

Figure 8. X-ray CT scan coupled with defect analysis software showcasing the internal voids in a PEEK 150PF sample. [Color figure can be viewed in the online issue, which is available at wileyonlinelibrary.com.]

with an analysis of void location bias and void morphology. Figures 7 and 8 demonstrate the void analysis results for PVDF and PEEK 150PF materials, respectively, with the defect analysis software highlighting internal voids of different volumes. The void volume fraction contained within each material directly affects permeability with higher void percentages leading to higher permeabilities.[27]

Figure 9 gives an overview of the internal void volume fraction in each material as measured via the X-ray CT defect analysis tool. Here, it is clear that the PVDF and VICTREX PEEK materials have the highest internal void percentages at between 3.0 and 4.0% of their total volume. This is followed by PA11 at around 1% void volume fraction, the EVONIK PEEK grades at $< 1\%$ and finally the PA12 grade with 0% voids detected. For the PVDF and VICTREX materials, this void percentage will affect permeability with significant scope for improvement via void removal techniques during processing. The PA12 material is the only one without any voids present and so represents the lowest permeation rate achievable for the material with the current production method. The average void radius is shown in Figure 10 with most materials giving values in the range between 200 and 300 μm.

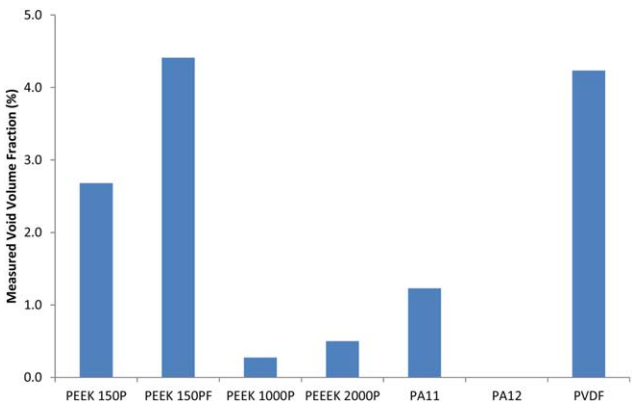

Figure 9. Void volume fraction results for each material tested for helium permeability. [Color figure can be viewed in the online issue, which is available at wileyonlinelibrary.com.]

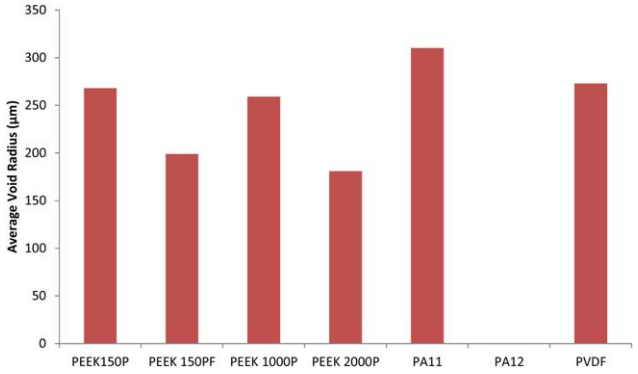

Figure 10. Average void radius results for each material tested for helium permeability. [Color figure can be viewed in the online issue, which is available at wileyonlinelibrary.com.]

Void volume size is shown in Figure 11, where the volume of voids ranges from 0.40 mm^3 down to 0.01 mm^3 for varying percentages of the total percentage of voids in each material. It can be seen here that the 1000P and 150PF materials have a higher percentage of smaller voids below 0.10 mm^3 while the PA11 for example, has a collection of larger voids above the 0.10 mm^3 mark. The void location bias has also been assessed with the defect analysis tool, whereby, Figure 12 shows the percentage of voids located through the thickness of a material from the mould surface on the left of the graph to the free side of the sample on the right of the graph.

The void content in rotationally moulded parts is influenced by a number factors but it is controlled by the applied heating cycle.[22,25] During the forming process, as the powder particles melt and coalesce together, the collapsing structure traps air beneath the surface in a pattern similar to that of the majority of materials tested here (PVDF, 1000P, 150P, and 150PF) with a higher distribution of voids located at the mould surface side of the sample. In these samples, the applied heating cycle has not allowed sufficient time for voids to diffuse into the polymer melt and so they have become trapped in the sample cross section.[39–41] Due to the viscosity of the polymer melt, the bubbles do not rise and so diffusion is the main method of void

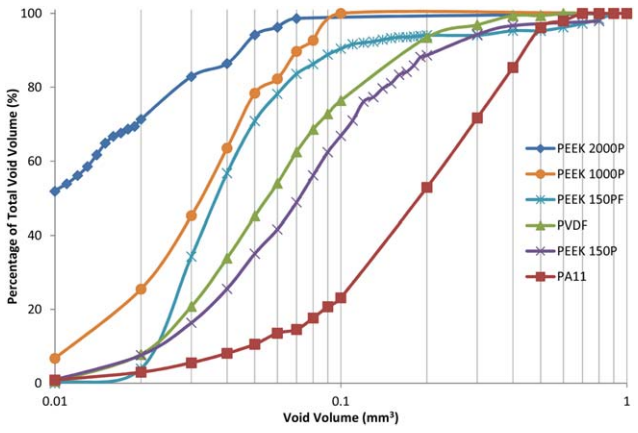

Figure 11. Graph displaying the percentage of total void volume versus the average void volume size for each material. [Color figure can be viewed in the online issue, which is available at wileyonlinelibrary.com.]

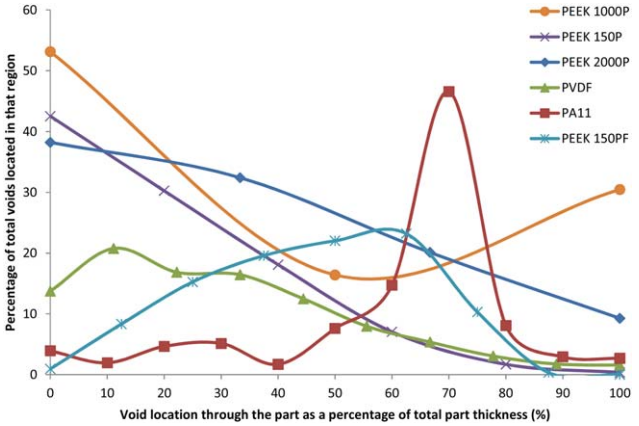

Figure 12. Percentage of total voids in the part versus the location of the voids as a percentage of the total part thickness (mould side on the left and free side on the right). [Color figure can be viewed in the online issue, which is available at wileyonlinelibrary.com.]

removal.[39–41] For the samples with void bias at a location closer to the free surface and minimal voids throughout the rest of the cross section, such as in the PA11 and 2000P materials, the heating cycle has provided enough time for the voids in these specific materials to diffuse into the melt (starting at the mould surface side closest to the heat source) but has still trapped air voids at locations nearer the free surface side.[24,39] An example of the bias of void locations is highlighted in Figure 13 where voids in a PA11 sample are clearly located in a region 3.0–4.0 mm from the mould surface at the bottom of the image.

The main drawback to the X-ray CT scanning used here is that the defect analysis only includes internal defects in its analysis. This is because the software needs to define the surface of the sample to distinguish between the solid material and surrounding air which removes surface voids from the analysis. This has led to lower predictions of void contents, specifically in the 1000P and 2000P materials, which are important for the permeability analysis, as will be shown.

While it is difficult to compare void statistics across different materials, certain conclusions can be drawn from a coupled analysis of the permeability results and void statistics. For the PVDF material, a reduction in the void content should lead to a further reduction in the permeability of the material. For the Nylon materials, PA11 is clearly the better permeation barrier as it maintains a lower permeation rate then PA12, even with a void volume fraction of 1%. A more comprehensive analysis of the effect of voids and internal defects can be carried out from an analysis of the PEEK materials tested. The void statistic results suggest that the EVONIK PEEK materials (1000P and 2000P) should have lower permeation rates due to their lower void contents, but this is not the case. In fact, the VICTREX PEEK grades (150P and 150PF) have a much lower permeability than the EVONIK PEEK grades (1000P ad 2000P), even with an almost 3% higher void content.

The 2000P material has a permeability coefficient of almost twice that of every other PEEK material tested. With an analysis of the X-ray CT images it can be seen somewhat in the 1000P material, and almost entirely in the 2000P material, that there are significant surface defects throughout the specimen, with Figure 14 highlighting a selection of these defects in a 2000P sample. These defects are 0.5–0.7 mm deep into both sides of the sample making up almost half of the specimen's overall thickness. These defects allow for higher rates of permeation by decreasing the effective thickness of the material and hence are the reason for the heightened rates of permeation. These surface defects have a substantial presence in the 2000P material and are the reason why the EVONIK PEEK materials have significantly higher permeabilities then the VICTREX PEEK materials. These defects are a direct result of poor powder consolidation during melting, with Figure 15 showing the presence of tail sections in the 2000P powder particles prior to specimen formation. These long fibrils and tails create larger air gaps throughout the sample during specimen formation which prevent proper consolidation of the powder during melting and hence increase permeability.

Leak Rate Comparisons for Varying Thicknesses

While it has already been shown that the leak rate is thickness dependent and thus the permeability coefficient is a better measure for ranking materials for permeability, the leak rate is still used to qualify COPV tanks and so it is the usual value quoted in COPV liner studies.[42,43] To this end, Fick's law, in conjunction with the permeability coefficient, has been used to predict the final leak rate of each liner material at a given pressure and thickness for a prospective COPV tank.

The envisaged use of the polymer materials studied is for a standard 90L cylindrical COPV tank with domed ends and a maximum allowable leak rate of 1×10^{-3} scc s^{-1} of helium at an operating pressure of 5 bar. If the tank has an internal surface area of around 1.1 m^2 then the maximum allowable leak

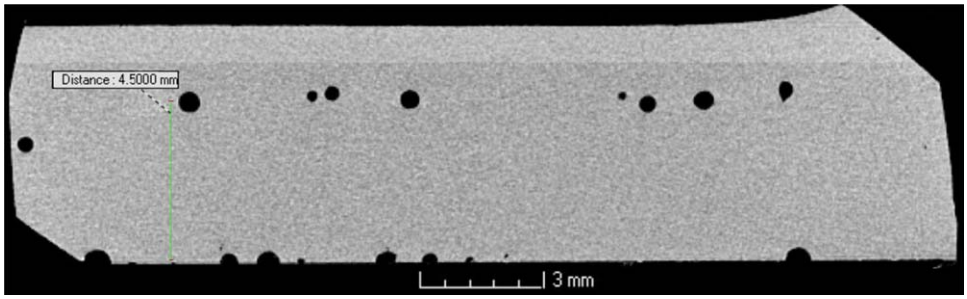

Figure 13. X-ray CT scans showing void location bias in a PA11 sample in a horizontal region around 3.0–4.0 mm away from the mould surface at the bottom of the image. [Color figure can be viewed in the online issue, which is available at wileyonlinelibrary.com.]

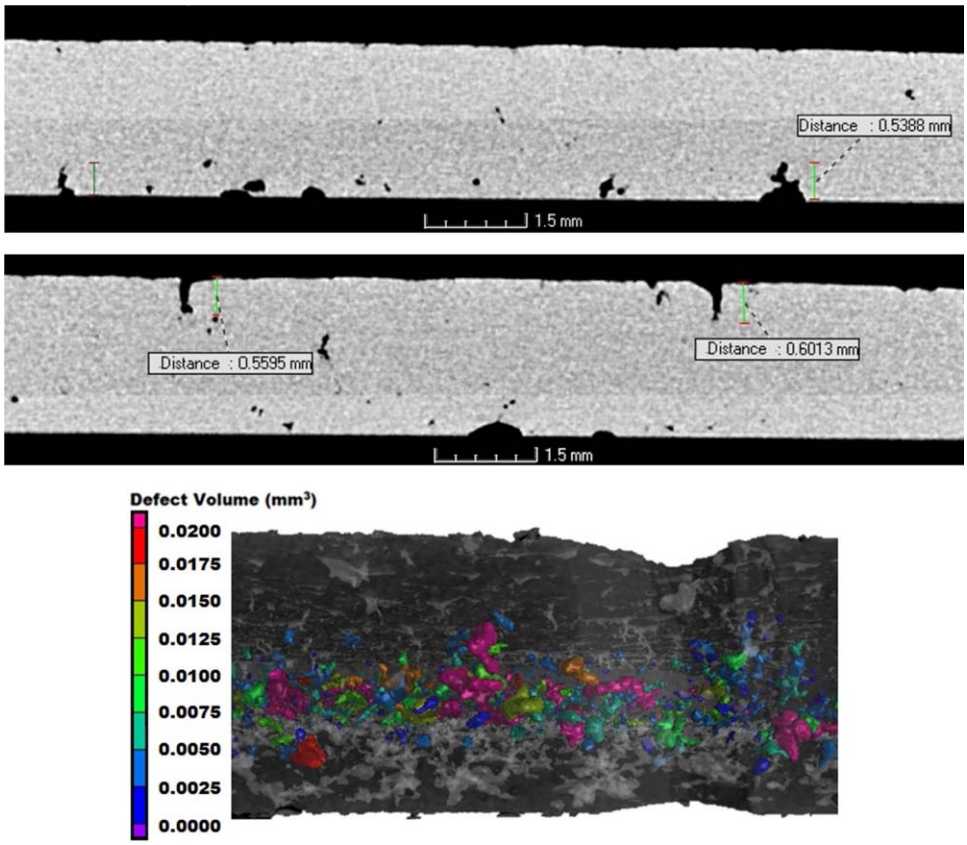

Figure 14. X-ray CT images and a transparent view of the internal defects in a PEEK 2000P samples showing thin cracks through the part thickness at both surfaces (mould surface along bottom of each image) along with the internal defect analysis highlighting the lack of surface defect incorporation at top and bottom surfaces. [Color figure can be viewed in the online issue, which is available at wileyonlinelibrary.com.]

rate of 1×10^{-3} scc s^{-1} divided by this surface area gives a maximum leak rate limit per m^2 area of 9.1×10^{-4} scc m^{-2} s^{-1}. Figure 16 shows the predicted effectiveness of each material at achieving this limit with different material thicknesses defined for a 5 bar pressure difference using Fick's law and the measured coefficients to predict the leak rate.

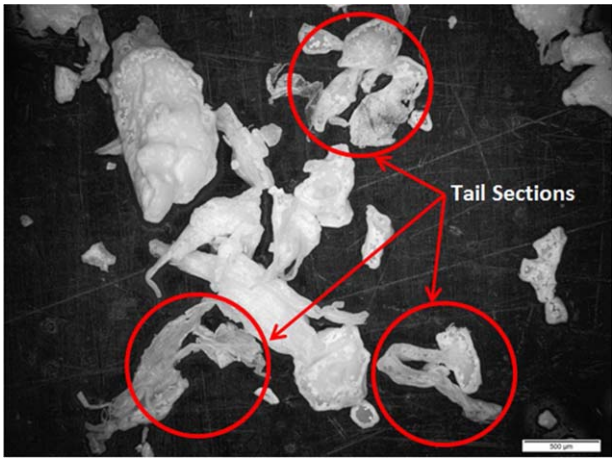

Figure 15. Optical microscopy image of the PEEK 2000P powder showing tail sections which inhibit intimate contact during melting and lead to larger void formations and defects. [Color figure can be viewed in the online issue, which is available at wileyonlinelibrary.com.]

This demonstrates that the PA11 and PVDF grades significantly outperform PA12 and PEEK with both materials displaying leak rates below that of the maximum allowable for a liner with a minimum thickness of 2.0 mm. A liner of twice this thickness at 4.0 mm is needed for the PEEK 150PF and PA12 materials to reach a sufficiently low leak rate to be acceptable as a liner material. At a 4.0 mm thickness, the PA11 and PVDF materials have reduced the leak rate further to less than half that of the

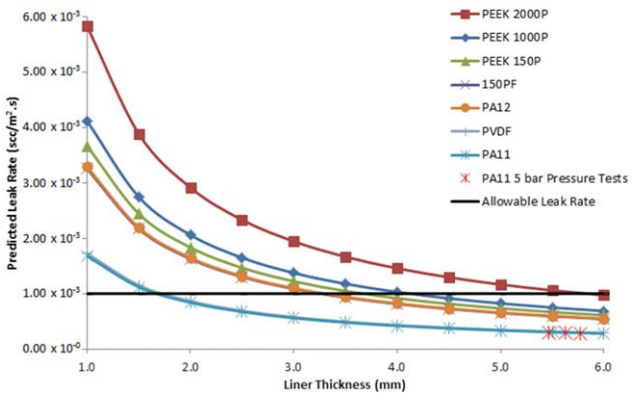

Figure 16. Leak rate predictions using Fick's Law and a standard pressure difference of 5 bar for different polymer liner thicknesses. [Color figure can be viewed in the online issue, which is available at wileyonlinelibrary.com.]

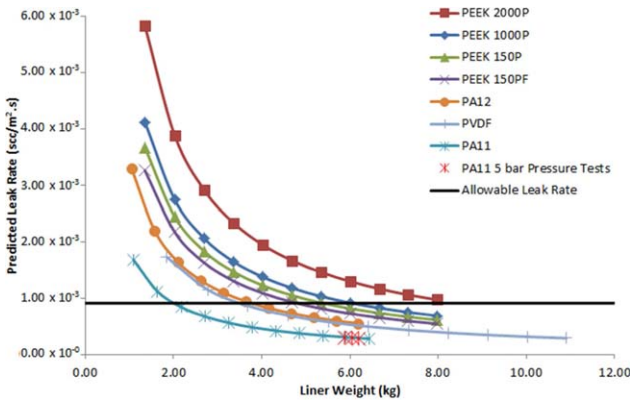

Figure 17. Leak rate predictions using Fick's Law and a standard pressure difference of 5 bar for different polymer liner weights. [Color figure can be viewed in the online issue, which is available at wileyonlinelibrary.com.]

allowable leak rate at an average of 4.25×10^{-4} scc m^{-2} s^{-1}, providing a significant factor of safety for the integrity of a prospective COPV tank. The 1000P, 2000P, and 150P grades eventually reach the maximum allowable limit at the 5.0 mm thickness mark but at this point their reduced performance lags significantly behind that of PA11 and PVDF.

The second effect of liner thickness which must be considered is the overall liner weight which is linked to the density of the specific polymer material tested. From Table I, it is clear that the Nylon materials are almost half as dense as PVDF which further separates the PA11 material from PVDF as the better material for low permeability liner applications and the lighter material for weight saving operations. A representation of the predicted liner weight versus the final leak rate has also been included in Figure 17 with results showing that a PA11 liner is far superior to all other materials on a weight basis as its leak rate is half that of all other materials for the same liner weight. This has been confirmed experimentally by further testing of three PA11 samples (with an average thickness of 5.6 mm) at a pressure difference of 5 bar (the expected operating pressure of the COPV designed here), the results for which have been included in Figures 16 and 17. The leak rate from these samples had an average value of 2.91×10^{-4} scc m^{-2} s^{-1} which is accurate to within 3% of the predicted value of 3.00×10^{-4} scc m^{-2} s^{-1}. This proves the accuracy of the permeability testing conducted here at a 1 bar pressure difference and further verifies that the PA11 material is the best barrier to permeation. The PVDF and PA12 are equal in regard to barrier properties for similar liner weights while the PEEK materials lag behind again for storage properties.

CONCLUSIONS

The viability of rotationally moulded polymers as low permeability COPV liner materials has been demonstrated via helium permeability testing, coefficient calculation and the use of Fick's law to predict specific leak rates for different liner thicknesses at a given pressure difference. The presence of air voids in the tested laminates has shown the effects of void contents on permeability while also demonstrating that significant void defects negatively affect barrier properties as demonstrated by the 2000P PEEK material.

X-ray CT scanning has given significant information in relation to void statistical data with void position data, void size, and void volume fraction data also assessed. This analysis has shown that for most materials the predominant location for voids is close to the mould surface, with the free side having a reduced void content showing the positional bias of voids in rotomoulded materials. It has also shown the effects of improper powder selection for rotational moulding trials as the lack of intimate powder contact leads to significant defect inclusion.

PA11 and PVDF have the highest barrier properties of all materials tested, with the lowest permeability coefficients and lowest predicted leak rates. Predicted leak rates with liner wall thicknesses above 2.0 mm with these polymers are lower than the maximum allowable leak rate for a 90L COPV tank operating at a 5 bar pressure difference. The predicted weight of a liner formed from each material has further separated PA11 from its counterparts as its weight savings far exceed that of PVDF. Permeability testing of PA11 samples, at a pressure difference of 5 bar, has verified these leak rate predictions for 5.6 mm thick samples which further proves the accuracy of the current test results. The availability of these materials in powder form makes them natural candidates for future trials as rotomoulded COPV liners for the storage of cryogenic fuels aboard rockets and satellites.

ACKNOWLEDGMENTS

The authors would like to thank the Irish Research Council (IRC) and the European Space Agency (ESA) for joint funding of this research under the Network Partnering Initiative (NPI) and for the use of facilities in ESA's ESTEC centre in Noordwijk. Research collaborators include ÉireComposites Teo, the Irish Centre for Composites Research (ICOMP), Airbus Defence & Space and Marine Renewable Energy Ireland (MaREI), the SFI Centre for Marine Renewable Energy Research–(12/RC/2302). They would also like to acknowledge the specific help and technical support provided by P.J. Feerick and Michael Flanagan of ÉireComposites Teo. Thanks also to Matrix Polymers, EVONIK and VICTREX for their help in supplying the materials for testing.

NOMENCLATURE

P	Permeability Coefficient (scc m^{-1} s^{-1} bar^{-1})
D	Diffusion Coefficient (m^2 s^{-1})
S	Solubility Coefficient (scc m^{-3} bar^{-1})
J	Leak Rate (scc m^{-2} s^{-1})
V	Total Volume of Gas (scc)
A	Area (m^2)
Δp	Pressure Difference (bar)
t	Time (s)
B	Thickness (m)
L	Time Lag (s)
C	Concentration (scc m^{-3})
V_f	Void Volume Fraction
R_v	Average Void Radius (μm)
T_m	Melt Temperature (°C)
x_c	Crystallinity (%)

REFERENCES

1. Mizutani, Y.; Sugimoto, S.; Matsuzaki, R.; Todoroki, A. *J. Acoustic Emission* **2009**, *27*, 89.
2. McLaughlan, P. B.; Grimes-Ledesma, L. R. NASA/SP–2011–57; Johnson Space Center: Houston, TX, **2011**.
3. Grimes-Ledesma, L. R.; Phoenix, S. L.; Beeson, H.; Yoder, T.; Greene, N. In ASC/ASTM 21st Annual Technical Conference of the American Society for Composites, Michigan, September 17-20, **2006**.
4. Thesken, J. C.; Murthy, P. L. N.; Phoenix, S. L.; Greene, N.; Palko, J. L.; Eldrigde, J.; Sutter, J.; Saulsberry, R.; Beeson, H. NASA/TM-2009-215684; Ohio Aerospace Institute: Brook Park, OH, **2009**.
5. Grimes-Ledesma, L. R.; Murthy, P. L. N.; Phoenix, S. L.; Glaser, R. In 9th Joint FAA/DoD/NASA Aging Aircraft Conference, Atlanta, GA, USA, March 6-9, **2006**.
6. Tam, W.; Hersh, M.; Ballinger, I. In 39th AIAA Propulsion Conference, Huntsville, AL, USA, July 20-23, **2003**.
7. Kawahara, G.; McCleskey, S. F. In 32nd AIAA/ASME/SAE/ASEE Joint Propulsion Conference. Lake Buena Vista, FL, USA, July 1-3, **1996**.
8. Tam, W. H.; Ballinger, I. In 42nd AIAA/ASME/SAE/ASEE Joint Propulsion Conference & Exhibit, Sacramento, CA, USA, July 9–12, **2006**.
9. Thesken, J. C.; Murthy, P. L. N.; Phoenix, S. L. NASA/TM-2009-215683; Ohio Aerospace Institute: Brook Park, OH, **2009**.
10. Tam, W. H.; Griffin, P. S.; Jackson, A. C. In 38th AIAA/ASME/SAE/ASEE Joint Propulsion Conference & Exhibit, Indianapolis, IN, July 7-10, **2002**.
11. Schultheiß, D. Ph.D. Dissertation, Universität Augsburg, Augsburg, Germany, **2007**.
12. Tam, W.; Ballinger, I.; Jaekle, D. E. Internal Report. ATK Space Systems Commerce Division, California, USA, **2008**.
13. Angelo, J. A. Space Technology; Greenwood Press: Westport, CN, USA, **2003**.
14. Labriet, M.; Poluet, L. AIAA SPACE 2013 Conference and Exposition, San Diego, CA, USA, September 10-12, **2013**.
15. Monson, L.; Moon, S. I.; Extrand, C. W. *J. Appl. Polym. Sci.* **2009**, *111*, 141.
16. Monson, L.; Moon, S. I.; Extrand, C. W. *J. Appl. Polym. Sci.* **2013**, *127*, 1637.
17. Amanat, N.; Nicoll, A. F.; Ruys, A. J.; McKenzie, D. R.; James, N. L. *J. Membr. Sci.* **2011**, *378*, 265.
18. Grimsley, B. W.; Cano, R. J.; Johnston, N. J.; Loos, A. C.; McMahon, W. M. In 33nd International SAMPE Technical Conference, Vol. *33*; Seattlle, WA, November 5-8, **2001**.
19. Herring, H. M. NASA/CR-2003-212422; Lockheed Martin Engineering & Sciences: Hampton, Virginia, **2003**.
20. Claudel, S.; Repellin, A.; Jaguenaud, L.; Lacour, D.; Bergerot, A.; Defoort, B. SAMPE Conference, Washington State Convention Center, Seattle, WA, USA, May 17-20, **2010**.
21. Mataloni, A. Internal Summary Report, AVIO - Comprensorio BPD, NTEESA10007 Issue 2, Italy, 2005.
22. Benedic, F.; Leard, J. P.; Lefloch, C. Report, EADS ST, St. Médard en Jalles, France, **2005**.
23. McEvoy, J. P.; Armstrong, C. G.; Crawford, R. *J. Adv. Polym. Tech.* **1998**, *17*, 339.
24. Crawford, R. J.; Kearns, M. P. Practical Guide to Rotational Moulding; Queen's University, Belfast, Rapra Technology Limited, **2003**.
25. ASTM D3418-15. ASTM International, West Conshohocken, PA, **2015**. DOI: 10.1520/D3418-15.
26. ASTM D1921-12. ASTM International, West Conshohocken, PA, **2012**. DOI: 10.1520/D1921-12.
27. Spence, A. G.; Crawford, R. J. *Proc. Instn. Mech. Eng. -B: B: J. Eng. Manufacture* **1996**, *210*, 521.
28. Spence, A. G.; Crawford, R. J. *Polym. Eng. Sci.* **1996**, *36*, 993.
29. Murray, B. R.; Leen, S. B.; Ó Brádaigh, C. M. *Proc. Instn. Mech. Engrs. Part L: J. Mater.: Designs Appl.* **2015**, *229*, 403.
30. ASTM D1434-82. ASTM International, West Conshohocken, PA, **2012**. DOI: 10.1520/D1434-82R09E01.
31. Umrath, W.; Fundamentals of Vacuum Technology; Oerlikon Leybold Vacuum Brochure: Cologne, Germany, **2007**.
32. Crank, J. The Mathematics of Diffusion, 2nd ed.; Brunel University, Clarendon Press: Oxford, UK, **1975**.
33. Extrand, B. W.; Monson, L. *J. Appl. Polym. Sci.* **2006**, *100*, 2122.
34. Cengel, Y. A. Heat and Mass Transfer: A Practical Approach, 3rd ed.; McGraw-Hill Companies Inc, New York, NY, USA, **2006**.
35. Brandrup, J.; Immergut, E. H.; Grulke, E. A. Polymer Handbook, 4th ed.; Wiley-Interscience, New York, NY, USA, **2003**.
36. Kanehashi, S.; Kusakabe, A.; Sato, S.; Nagai, K. *J. Membr. Sci.* **2010**, *365*, 40.
37. Guinault, A.; Sollogoub, C.; Ducruet, V.; Domenek, S. *Eur. Polymr. J.* **2012**, *48*, 779.
38. McGonigle, E. A.; Liggat, J. J.; Pethrick, R. A.; Jenkins, S. D.; Daly, J. H.; Hayward, D. *Polymer* **2001**, *42*, 2413.
39. Crawford, R. J.; Throne, J. L. Rotational Molding Technology; William Andrew Publishing: New York, **2002**.
40. Gogos, G. *Polym. Eng. Sci.* **2004**, *44*, 388.
41. Kontopoulou, M.; Vlachopoulos, J. *Polym. Eng. Sci.* **1999**, *39*, 1189.
42. Robinson, M. J.; Eichinger, J. D.; Johnson, S. E. In 43rd AIAA/ASME/ASCE/AHS/ASC Structures, Structural Dynamics, and Materials Conference, Colorado, USA, April 22-25, **2002**.
43. Robinson, M. *J. J. Spacecr. Rockets* **2008**, *45*, 82.